Energy Efficiency Analysis of Coupled Thermal Radiation and Free Convection within a Square Enclosure with Internal Heating

AKRAM MAZGAR, FADHILA HAJJI, FAYCAL BEN NEJMA
EMIR Laboratory, University of Monastir,
The Preparatory Institute for Engineering Studies of Monastir,
Ibn Eljazar Street, Monastir 5019,
TUNISIA

Abstract: - This study explores the simultaneous impact of thermal radiation and free convection within a square cavity featuring internal heating. The walls are consistently held at a stable temperature through isothermal cooling, while an internal heat source sustains a consistently higher temperature. The radiation component is characterized by employing the FT_{40} discrete-ordinate approximation in conjunction with the statistical narrow-band correlated-k method (SNBcK). The primary focus lies in discerning the influences of radiation on both flow patterns and heat transfer. Particular emphasis is placed on investigating energy efficiency and its correlations with key governing parameters, including the heat source temperature, wall emissivity, and the size and placement of the heater. A noteworthy revelation from this analysis is the substantial impact of radiation on the acceleration of vortices, leading to a homogenizing impact on temperature distributions. Additionally, it is observed that the highest level of energy efficiency is realized by siting the heater at the central lower section of the enclosure.

Key-Words: - Energy efficiency, Natural convection, Radiation, Heat source, SNBcK, square cavity.

Received: April 29, 2023. Revised: October 9, 2023. Accepted: November 28, 2023. Published: December 31, 2023.

1 Introduction

The effects of combined thermal radiation and convection within enclosures have emerged as a significant concern across various industries, impacting applications such as heat exchangers, boilers, thermal insulation systems, nuclear reactor systems, burners, combustion chambers, and metallurgical processes. Notably, enclosures featuring internal heating have garnered substantial attention due to their relevance in numerous heat transfer processes and their implications in various fields, including thermal engineering, culinary arts, materials science, appliance safety, improvement of industrial processes, heating device design such as ovens, microwaves, water heaters, and other practical applications. In-depth comprehension enables the optimization of heat distribution, and improvement of energy efficiency, and ensures uniform cooking or heating. In such applications, Heat transfer through thermal radiation and free convection play pivotal roles in energy exchanges. In these processes, maximizing energy efficiency is fundamental, requiring the identification of ideal configurations that provide the best heat transfer performance, [1], [2]. Research in this area led to several publications, highlighting the significance of understanding the interaction between radiation and convection to increase system performance. For instance, [3] inspected the free convection flow in a square enclosure having an internal heater. Their findings underlined that the region where heat transfer is focused is located in the lower region of the heated surface area. In [4], the authors presented a numerical simulation dealing with the interaction of radiation with convection and conduction within the confined volume of a square-shaped cavity containing a heat generation source. Their results specified that wall-to-wall heat transfer meets resistance from the heated block. Additionally, [5], performed a numerical investigation of combined radiation-free convection heat transfer in a titled enclosure that included a centrally positioned inner source. Their findings indicated that the inclination angle had a diminishing impact on heat transfer within the enclosure, particularly when thermal radiation was present. In a distinct investigation, [6], delved into the characteristics of free convection within a cooled square-shaped enclosure including an isothermal cylindrical heat source. Their comments highlighted that the development of convection cells was significantly influenced by the location of the heater and the Rayleigh number. Furthermore, [7], presented the impact of the heater size localized at the center of a square enclosure on

fluid structure and heat transfer characteristics. Their study reveals the specific importance of understanding in what way the heater size marks both heat transfer and the structure of the fluid flow. [8], tested the influence of surface-to-surface radiation on the disruption of natural convective flows through a square cavity comprising a centrally situated, heated inner body. Their results specified that the radiative contribution raises the Rayleigh number, principally during the initial transition to the transitional regime. [9], used the lattice Boltzmann approach to examine the free convection of nanofluid around a horizontal circular cylinder within a square cavity. They noted that, in contrast to the Hartmann number, both mean Nusselt and Rayleigh numbers exhibit a rise as the volume fraction of the nanoparticle increases. [10], investigated the impact of the heater location on entropy creation resulting from mixed convection within an open square enclosure. [11], studied heat transfer, taking into account the interplay between surface radiation and free convection in a square cavity with a heated plate positioned at the center. They highlighted that thermal radiation leads to improved temperature homogenization within the enclosure. Additionally, they demonstrated that the contribution of convective heat transfer decreases with emissivity when the plate is vertically located, but increases when the plate is positioned horizontally. [12], performed a numerical investigation on free convection within a differentially heated enclosure with volumetric heat generation. Their findings indicated that a horizontal magnetic field proved to be the most effective in stabilizing the flow. In another numerical study, [13], inspected the impact of thermal radiation and internal heating on mass and heat transfer over an upward-facing horizontal flat plate within a porous medium containing a nanofluid. They concluded that thermal radiation significantly enhances flow velocity, as well as the profiles of temperature and nanoparticle volume fraction. [14], investigated laminar free convection in an inclined enclosure featuring a centrally heated body. Their results revealed that elevating the inclination angle of the cavity leads to the suppression of heat transfer throughout the cavity. In a numerical simulation, [15], the unsteady characteristics of free convection within a square enclosure with various heat source configurations at the bottom wall were explored. Notably, they observed that reducing the heat source length resulted in a decrease in the heat generation rate. In other studies, [16], [17] delved into the analysis of generated irreversibility arising from natural convection within a square enclosure featuring an internal cylindrical heat source. Their observations indicated a substantial increase in entropy creation rates attributed to heat transfer and fluid friction with an elevated Rayleigh number. [18], conducted an extensive review of numerical and experimental investigations related to free convection phenomena in rectangular or square cavities, both with and without an internal heat source. Moreover, [19], explored convective-radiative energy transport in a titled enclosure featuring an energy-generating body. Their findings highlighted that the influence of radiation on overall thermal transmission becomes significant with an increase in surface emissivity. [20], analyzed free convection in a square enclosure containing a circular heater subjected to nanoparticles and a magnetic field. They concluded that the heating rate primarily increases with a rise in the Rayleigh number and inversely with a diminution in the Hartmann number. In [21], the authors studied a numerical investigation on free convection combined with surface radiation within a square enclosure filled with air and including two heat generating elements. They showed the influence of the conductivity ratio, the Rayleigh number, and the emissivity on the heating process and fluid flow structure. In a three-dimensional numerical investigation, [22], explored entropy creation under thermal convection in a cubic cavity comprising a heater source. They revealed that their findings carry significant implications for the optimization and design of heat transfer processes. Recently, [23], explored the impact of a heat source on hybrid nanofluids using the heatline approach. Their findings indicated direct proportionality between the heater length and the Nusselt number. On a related note, [24], conducted an analytical study on steady free convection in a vertical rectangular enclosure resulting from uniform volumetric heating. The study incorporated two pairs of heat sources/sink within a vertical rectangular enclosure. Their results demonstrated a notable agreement in terms of isotherms, streamlines, and temperature and velocity distributions.

An examination of the chosen bibliography highlights that there exist various industrial setups where the impact of volumetric radiation on fluid flow and heat transfer has not been sufficiently explored. The primary objective of this paper is to conduct a numerical investigation into the impact of volumetric radiative heat transfer on laminar free convection within an isothermally heated square enclosure featuring an internal heat source. Additionally, particular emphasis is placed on analyzing energy efficiency to delineate the optimal

configuration that yields the most effective heat transfer performance.

2 Problem Formulation

This study focuses on a 2D square enclosure as the physical model, incorporating an internal local heat source and diffusive grey radiating walls. The selected working fluid for the study is superheated steam, identified as a non-grey medium with emitting-absorbing properties and devoid of scattering, as illustrated in Figure 1. Note that the fluid motion is presumed to be steady, laminar, and compressible. Moreover, the walls of the enclosure are kept at a consistently low temperature (T_c), while the internal heater operates at an elevated temperature (T_h). To scrutinize the characteristics of fluid flow and heating process, we utilized a numerical computation with COMSOL Multiphysics, concurrently conducting an iterative coupled simulation through Matlab software.

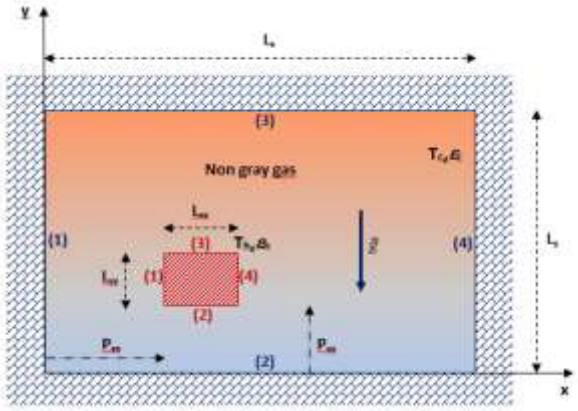

Fig. 1: Geometry of the enclosure with an internal heater

Considering the specified assumptions detailed above, the governing equations are provided as follows:

$$\nabla.(\rho\vec{u}) = 0 \quad (1)$$

$$\rho(\vec{u}.\nabla).\vec{u} = \nabla.\left[-P\bar{\bar{I}} + \mu(\nabla\vec{u} + (\nabla\vec{u})^T) - \frac{2}{3}\mu(\nabla\vec{u})\bar{\bar{I}}\right] + \overrightarrow{F_B} \quad (2)$$

where $\overrightarrow{F_B}$ denotes the force of buoyancy, it is given by Archimedes' principle and can be expressed as:

$$\begin{cases} F_{Bx} = -\rho g \sin\theta \\ F_{By} = -\rho g \cos\theta \end{cases} \quad (3)$$

$$\rho C_p \vec{u}.\nabla T = \nabla.(\lambda\nabla T) - div(\overrightarrow{q_r}) \quad (4)$$

Certainly, the radiative source term given in Equation (4) symbolizes the radiation contribution within the medium.

For the convection governing equations, the pertinent boundary conditions are specified as the following:

- On cavity walls: $T = T_c$
- On heater walls: $T = T_h$
- On all walls: $u_x = u_y = 0$

Assuming isothermal walls, the boundary conditions for thermal radiation are specified as follows:

$$I_\nu^i(\vec{\Omega}) = \varepsilon_w I_\nu^b(T_w) + \frac{1-\varepsilon_w}{\pi}\int_{\vec{\Omega}'/\vec{\Omega}'.\vec{n}<0} I_\nu^i(\vec{\Omega}')\,\vec{\Omega}'.\vec{n}\,d\Omega' \quad (5)$$

The radiation code is developed based on the FT40 discrete-ordinate approximation. This technique entails discretizing the angular space into a finite set of ordinates or directions. The radiative transfer equation (RTE) is resolved numerically for each direction.

Furthermore, the SNBcK model allows determining the radiative characteristics of superheated steam. This method is based on the extraction of the gas spectral absorption coefficients from the corresponding transmissivities.

Please note that the radiation code is established based on the FT_{40} discrete-ordinate approximation. Therefore, the RTE can be expressed according to equation (6):

$$\frac{dI_\nu^i(l,\vec{\Omega})}{dl} = -\kappa_\nu^i(l) I_\nu^i(l,\vec{\Omega}) + \kappa_\nu^i(l) I_\nu^b(T) \quad (6)$$

It is worth emphasizing that the SNBcK approach is associated with the 4-point Gauss-Legendre quadrature to compute the radiative source term which is expressed following Eq. (7), [25], while the net radiative flux is given in Eq. (8), [26], [27].

$$div(\overrightarrow{q_r}) = \sum_{bands}\int_{4\pi}\sum_{i=1}^{4} w^i \kappa_\nu^i \left(I_\nu^b - I_\nu^i(\vec{\Omega})\right) d\Omega\Delta\nu \quad (7)$$

$$q_r = \sum_{bands}\int_{4\pi}\sum_{i=1}^{4} w^i I_\nu^i\left((\vec{\Omega})\right)\vec{\Omega}.\vec{n}\,d\Omega\Delta\nu \quad (8)$$

Note that COMSOL Multiphysics allows delivering the thermo-physical properties of the working fluid supposed to be an ideal gas. The application of this model within the temperature range of 380 to 850°C ensures that the simulated physical properties align with the expected behavior of the working fluid within this specific temperature

interval. Moreover, a linear extrapolation was used to estimate values outside the given range.

In order to enhance comprehension of the heat exchange at different points on the walls, which is essential for estimating the overall heating process in the system, we give the formulas of the local convection and radiation Nusselt numbers at walls, respectively:

$$Nuc(x\ or\ y) = \frac{2(L_xL_y - L_{xx}L_{yy})}{L_x+L_y+L_{xx}+L_{yy}} \frac{1}{(T_h-T_c)} \left|\frac{\partial T}{\partial(y\ or\ x)}\right|_{\mathrm{w}} \quad (9)$$

$$Nur(x\ or\ y) = \frac{2(L_xL_y - L_{xx}L_{yy})}{L_x+L_y+L_{xx}+L_{yy}} \frac{|q_r|}{\lambda(T_{\mathrm{w}})(T_h-T_c)} \quad (10)$$

Certainly, computing the mean Nusselt number for each of the eight surfaces involves averaging the local Nusselt.

$$\overline{Nu} = \frac{1}{L_{x,xx,y\ or\ yy}} \int_0^{L_{x,xx,y\ or\ yy}} Nu(x, xx, y\ or\ yy) d(x, xx, y\ or\ yy) \quad (11)$$

In addition, the average temperature and average velocity can be calculated as follows:

$$\begin{cases} T_a = \frac{1}{L_xL_y - L_{xx}L_{yy}} \iint_{surface} T(x,y)dydx \\ u_a = \frac{1}{L_xL_y - L_{xx}L_{yy}} \iint_{surface} \sqrt{u_x^2(x,y) + u_y^2(x,y)}dydx \end{cases} \quad (12)$$

To make the heating process more effective, we defined the corresponding energy efficiency as the ratio between the temperature increase resulting from heat transfer and the necessary heat flux to achieve this temperature rise. It is expressed as follows:

$$E = \frac{\frac{T_a - T_c}{T_h - T_c}}{\sum_{j=1}^{4}(\overline{Nuc}_{o,j} + \overline{Nur}_{o,j})} \quad (13)$$

3 Numerical Procedure and Validation

Let's reiterate that we used a combination of Matlab and COMSOL Multiphysics for simulating heat transfer and fluid flow. In fact, COMSOL Multiphysics® employs finite element analysis as a general computational method for resolving the governing equations with Matlab handling parameter initialization and storage.

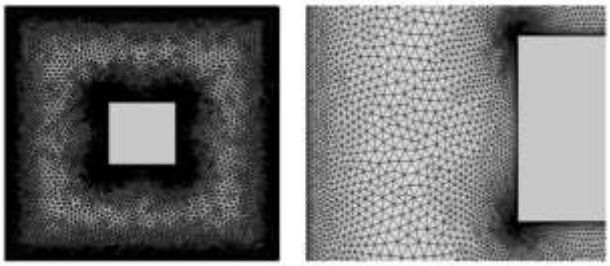

(a) (b)

Fig. 2: The computation mesh (a) inside the cavity; (b) in vicinities of walls

T_c=400K; T_h=800K; L_y=L_x=0.1m; L_{yy}= L_{xx} =0.025m; ε_c=ε_h=1; P=1atm, P_{yy}=P_{xx}= 0.0375m

The use of an adaptive mesh in COMSOL Multiphysics®, along with the information on the total number of mesh elements and boundary elements represents a dynamic feature that refines the mesh in specific zones where higher resolution is needed (Figure 2). The total number of mesh elements is 25,386 whereas the number of boundary elements is 852.

Note that the validation of the COMSOL code was achieved by using the Rayleigh-Bénard convection within a square cavity of an "L" edge with two insulating vertical surfaces. The upper wall is maintained at a consistently lower temperature (T_c), while the bottom one is consistently held at a higher temperature (T_h). In the spirit of validating our convection model, we established the local distributions of the Nusselt number at the active wall, as shown in Figure 3. In fact, the comparison of our results and those of the article, [28], shows good agreement with an error rate not exceeding 2%. This proves that our code is providing accurate and reliable simulations for the Rayleigh-Bénard convection case.

For the purpose of validating our radiative model, we conducted some computations to juxtapose outcomes derived from the SNBcK-based band model with data accessible in the existing literature. To achieve this, a physical model was employed, featuring a rectangular enclosure with dimensions of 1 m × 0.5 m, housing water vapor at a temperature of 1000 K, and enclosed by black walls maintained at a temperature of 0 K. The distributions of the radiative source term given in Figure 4, compare our current findings using the S_8 quadrature and those documented by [29], using the T_7 quadrature. The findings reveal a significant alignment between the two investigations and the error perceived does not exceed 3%, indicating a high level of concordance.

Moreover, as indicated in Table 1, employing a spaced grid with dimensions 40*40 demonstrates a judicious compromise to ensure precise accuracy calculations.

Furthermore, the local distributions of the radiative heat flux kept at the upper enclosure wall were established to determine the suitable quadrature model, as illustrated in Figure 5. It is noteworthy to mention the distortions present in the respective trends due to the ray effect resulting from the selected angular discretization approach. The decision was made in favor of employing the FT_{40} with a substantial number of directions to mitigate the influence of the ray effect, [30].

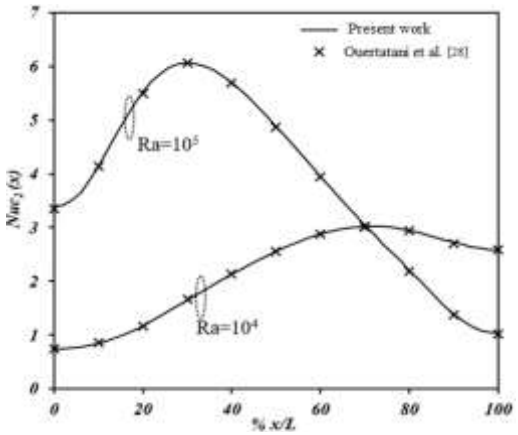

Fig. 3: Validation of the convective model
T_h=800K; T_c=400; P=1atm; $L_y = L_x = 0.1$m

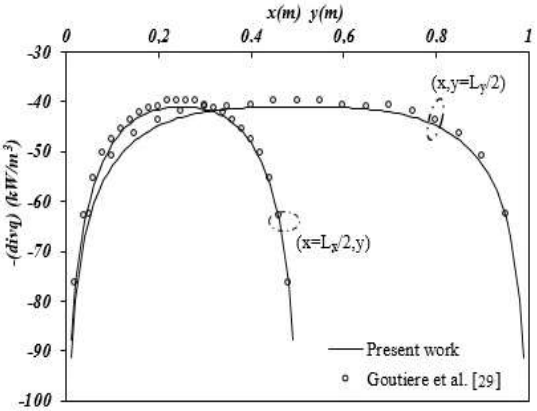

Fig. 4: Validation of the radiative model
T_0=1000K; T_W = 0; P_0 =1atm; $\varepsilon_h=\varepsilon_c=1$; L_x = 1m; L_y =0.5m

Table 1. Grid sensitivity test (case of pure radiation)
T_h=800K; T_c=400K; P=1atm; $\varepsilon_c=\varepsilon_h=1$; $L_y=L_x=0.1$m; $L_{yy}=L_{xx}=0.025$m; $P_{yy}=P_{xx}=0.0375$m

Grid x*y	Average radiative Nusselt numbers at the cavity walls			Average radiative Nusselt numbers at the heaters walls		
	$Nur_{1,4}$	Nur_2	Nur_3	$Nur_{1,4}$	Nur_2	Nur_3
24*24	36.254	33.043	38.915	66.080	66.639	63.734
32*32	36.159	33.076	38.995	65.999	66.591	63.712
40*40	36.102	33.080	39.014	66.006	66.724	63.773

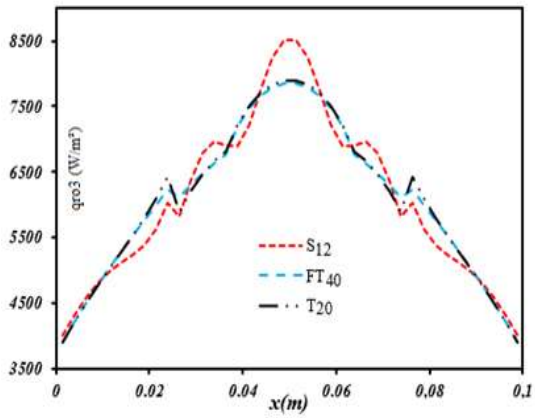

Fig. 5: Quadrature effect
T_h=800K; T_c=400K; P=1atm; $\varepsilon_c=\varepsilon_h=1$; $L_y=L_x=0.1$m; $L_{yy}=L_{xx}=0.025$m; $P_{yy}=P_{xx}=0.0375$m

4 Problem Solution

The primary characteristics of thermal radiation's impact on the heating process and convective flow within a square enclosure containing an internal heat source are delineated in Figure 6, Figure 7, Figure 8, Figure 9, Figure 10, Figure 11, Figure 12, Figure 13 and Figure 14. Examining the local velocity distributions depicted in Figure 6(a), the flow pattern reveals two symmetrical counter-rotating convective cells distributed throughout the entire domain. Notably, the buoyant thermal plume extends over the upper boundary of the enclosure, with the maximum flow velocity attained near this zone and near the upper corners of the heater. Moreover, the boundary layer beneath the heat source experiences destabilization due to vortices generated above the heater, leading to thermal stratification in the region between the heater and the bottom surface of the enclosure, resulting in low fluid velocities. It is crucial to highlight that thermal radiation significantly contributes to heat transfer and flow characteristics, as illustrated in Figure 6(b). The presence of radiation amplifies temperature profiles, resulting in more developed

and deformed cells that occupy a larger portion of the cavity space. Additionally, water vapor particles exhibit noticeable acceleration near the upper wall of the enclosure. Furthermore, local variations in the source term resulting from the radiative contribution are presented in Figure 6(c). It is crucial to underscore that regions with a negative radiative source term are located in proximity to the upper wall of the enclosure and above the heat source, where the hottest particles are concentrated.

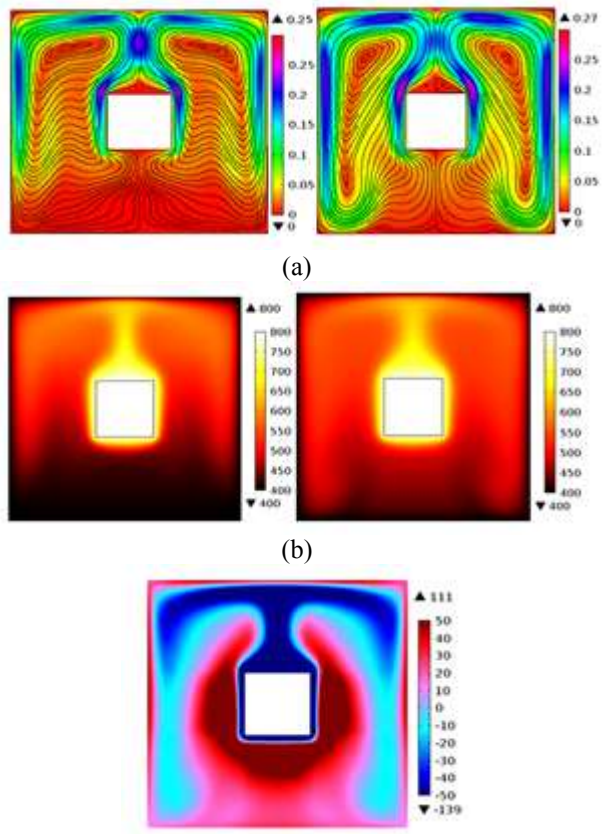

(a)

(b)

(c)

Fig. 6: Local distributions without radiation (left); with radiation (right)
(a) velocity fields (m/s); (b) temperature fields (K); (c) radiative source term (kWm^{-3});
T_h=800K; T_c=400K; P=1atm; $\varepsilon_c=\varepsilon_h=1$; $L_y=L_x$=0.1m; $L_{yy}=L_{xx}$=0.025m; $P_{yy}=P_{xx}$=0.0375m

4.1 Impact of the Heater Temperature

The heater temperature effects on average distributions are depicted in Figure 7. It is noteworthy that, independently of the radiative impact, the average temperature exhibits a nearly linear profile. Furthermore, an increase in the heater temperature significantly elevates the mean values of the gas temperature and the flow rate. Conversely, even at relatively lower heat source temperatures, it can be inferred that volumetric radiation contributes to achieving a more uniform temperature, causing a substantial change in flow despite the mean temperature remaining almost constant. Figure 7(c) illustrates the distribution of mean convection Nusselt numbers along the cavity boundaries based on the heater temperature. It should be observed that in the absence of radiation, the convection Nusselt number along the bottom surface of the cavity maintains a nearly constant profile, approaching practically null values. This is attributed in part to the retention and immobilization of fluid particles beneath the heating element. Moreover, the mean convective Nusselt numbers of the upper and side walls of the enclosure exhibit increasing trends, prominently visible in the $\overline{Nuc}_{o3}$ profile. The buoyancy force escalates with an increase in the temperature of the heating element, resulting in significant temperature gradients near the upper surface. This, in turn, enhances convective heat exchange between this wall and the gas. Additionally, when considering the influence of radiation, the average convective Nusselt number along the upper surface remains nearly constant, whereas those computed at the bottom and side walls distinctly show substantial and amplified profiles. In this scenario, fluid particles near the bottom and side walls experience acceleration, thereby improving heat transfer between these surfaces. Figure 7(d) illustrates the influence of the heater temperature on average convection Nusselt numbers along the heat source walls. It is noteworthy that an elevation in the heat source temperature results in a reduction in the corresponding Nusselt numbers, displaying a quasi-linear profile for those computed at the upper wall. Furthermore, the radiative contribution demonstrates no significant impact on convection heat exchange near the heater walls, presenting a slight amplification in the profile of the Nusselt number along the upper wall and a minor attenuation in those computed at the other walls.

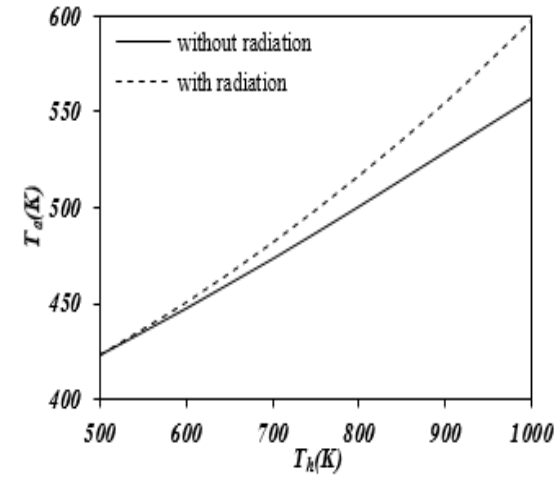
without radiation
with radiation
$T_o(K)$
$T_h(K)$

(a)

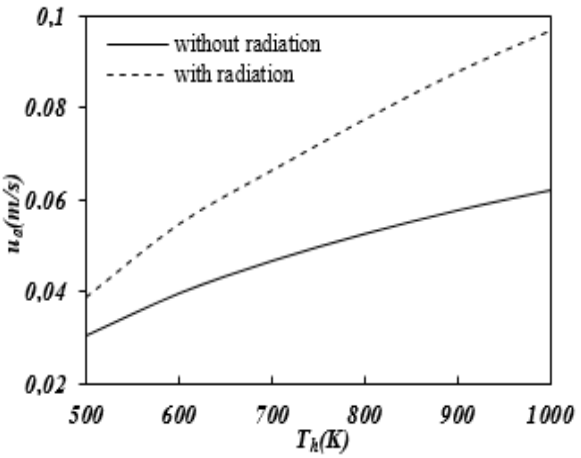
without radiation
with radiation
$u_o(m/s)$
$T_h(K)$

(b)

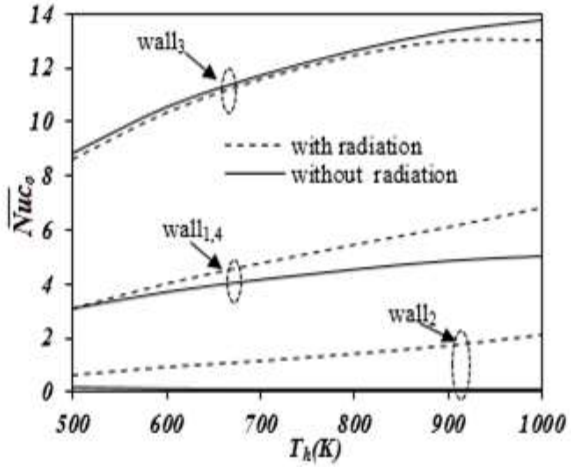
wall$_3$
with radiation
without radiation
wall$_{1,4}$
wall$_2$
$\overline{Nuc_o}$
$T_h(K)$

(c)

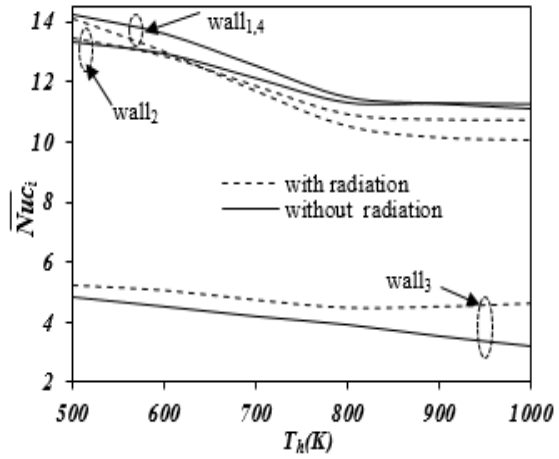
wall$_{1,4}$
wall$_2$
with radiation
without radiation
wall$_3$
$\overline{Nuc_i}$
$T_h(K)$

(d)

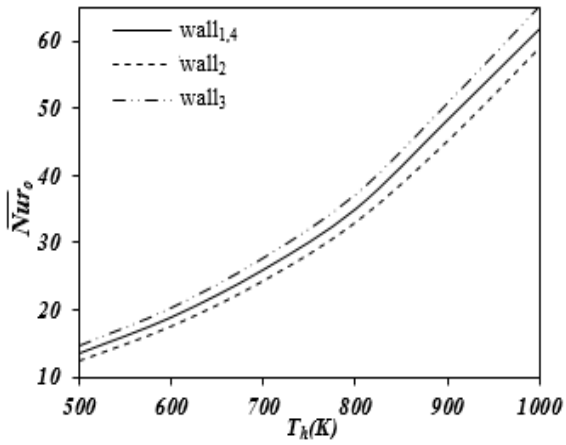
wall$_{1,4}$
wall$_2$
wall$_3$
$\overline{Nur_o}$
$T_h(K)$

(e)

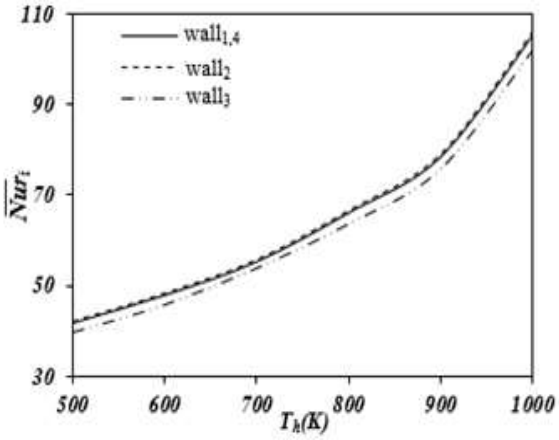
wall$_{1,4}$
wall$_2$
wall$_3$
$\overline{Nur_i}$
$T_h(K)$

(f)

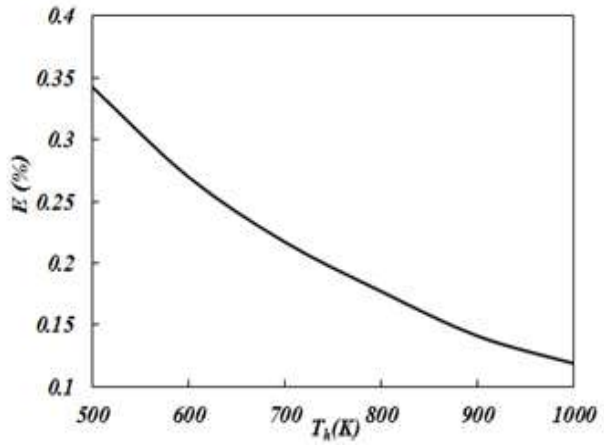

(g)

Fig. 7: The influence of the heater temperature on average distributions
T_c=400K; P=1atm; $\varepsilon_c=\varepsilon_h=1$; $L_y=L_x$=0.1m; $L_{yy}=L_{xx}$=0.025m; $P_{yy}=P_{xx}$=0.0375m

The data presented in Figure 7(e) and Figure 7(f) delineate the distribution of mean radiation Nusselt numbers at each wall based on the temperature of the heater. Notably, the corresponding profiles exhibit increasing trends characterized by quasi-exponential curves. In Figure 7(g), the impact of the heater temperature on energy efficiency is demonstrated. It is evident that raising the temperature of the heater diminishes energy efficiency. In such conditions, a notable energy loss is observed through surface-to-surface exchanges that do not contribute to the temperature rise of the gas.

4.2 Influence of the Heater Emissivity

Figure 8 depicts the emissivity impact of the enclosure walls on average distributions. It is noteworthy that an increase in emissivity results in higher heat losses due to radiation at the enclosure surfaces and reduces their reflectivity, consequently decreasing fluid-fluid heat exchange in favor of fluid-wall heat transfer. As depicted in Figure 8(a) and Figure 8(b), lower wall emissivity leads to an increased reflection of thermal radiation originating from the heat source. This enhancement in reflection creates additional chances for heating the gas. In the case of a perfectly emissive wall, this translates to the absorption of radiation from the heater upon first contact with the surface. Conversely, when dealing with a perfectly reflective wall, radiation reflects until it reaches the heating element, facilitating heat exchange and consequently elevating the average temperature of the gas, while the mean velocity remains relatively constant. Another noteworthy point highlighted in Figure 8(c) and Figure 8(d) is that elevating the emissivity of the cavity surfaces increases the mean convection Nusselt numbers along the heater boundaries compared to those calculated along the cavity surfaces. Furthermore, increasing the emissivity of the cold walls reduces the radiation emitted from the heater, thus enhancing heat transfer between the heater and the gas. However, this results in reduced temperature gradients at the cold surfaces, leading to a decrease in mean convection Nusselt numbers along the cavity surfaces. Conversely, increasing the emissivity of the enclosure walls amplifies temperature gradients near the heat source surfaces, consequently raising the corresponding mean convection Nusselt numbers. Figure 8(e) and Figure 8(f) show variations of the mean radiation Nusselt numbers based on the emissivity of the enclosure walls. As anticipated, the corresponding Nusselt numbers increase significantly with higher emissivity of the cavity walls, attributed to a sustained increase in radiative heat flux. In Figure 8(g), an increasing profile of energy efficiency is presented according to wall emissivity. Decreasing the emissivity of the cavity walls reduces heat transfer between surfaces, thereby enhancing gas-gas heat transfer at the expense of heat transfer between surfaces.

4.3 Effect of the Heater Size

The influence of the heater aspect ratio on the flow structure is depicted in Figure 9, showcasing the variation of the heater length (L_{yy}) while maintaining the corresponding width (L_{xx}). Reducing the heater size increases the flow rate within the plume while preserving its structure. Turning to the temperature distribution presented in Figure 10, the plume appears thinner and more confined above the heater, exhibiting a noticeable increase in cold zones below the heater.

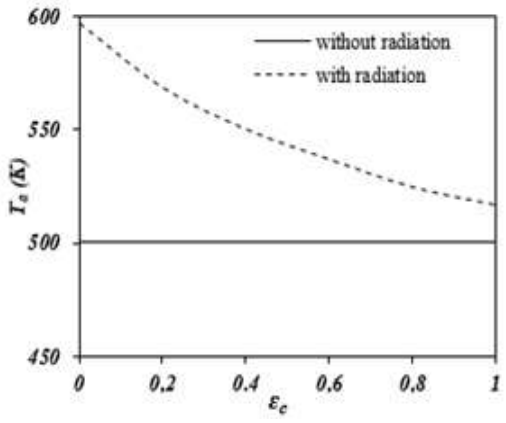

(a)

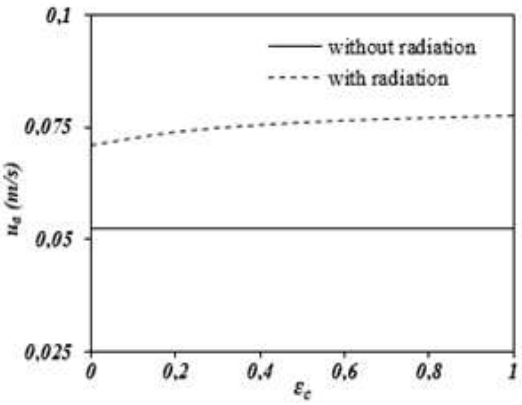

(b)

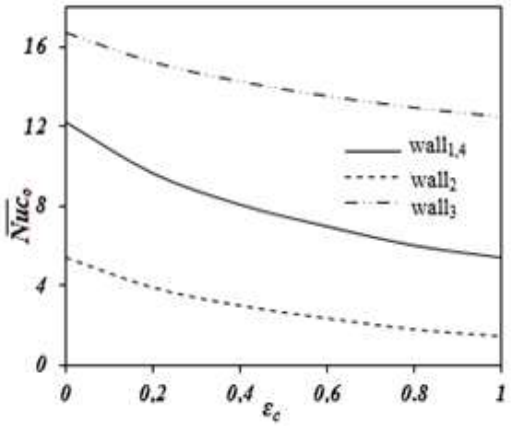

(c)

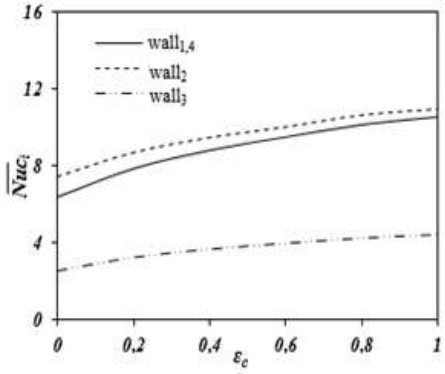

(d)

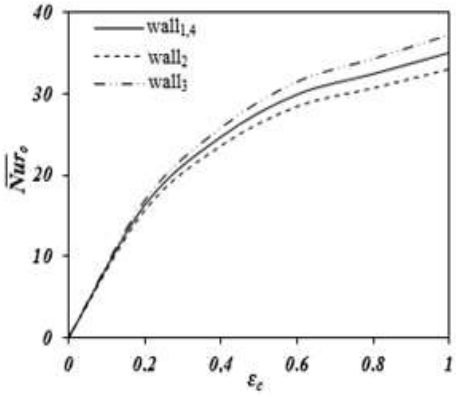

(e)

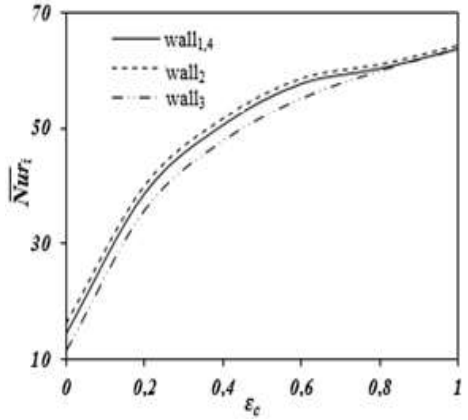

(f)

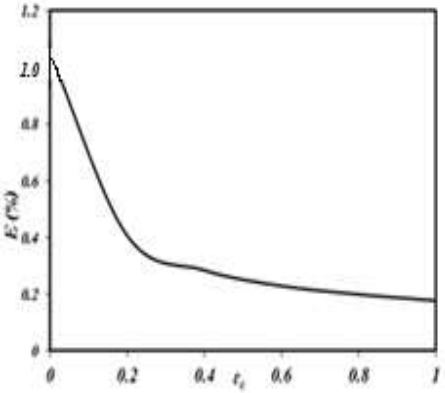

(g)

Fig. 8: Impact of the wall emissivity on the mean distributions
T_h=800K; T_c=400K; P=1atm; ε_h=1; L_y=L_x=0.1m; L_{yy}=L_{xx}=0.025m; P_{yy} =P_{xx}=0.0375m

It is noteworthy to mention a decrease in the mean temperature of the fluid particles situated above the heater due to the reduction in heat transfer between surfaces resulting from the smaller heater size. Additionally, a notable increase in the plume width is observed under the influence of the radiative contribution, particularly in areas below the heater that are primarily involved in heat exchange. This is anticipated given the downward extension of the cells, but it also leads to an augmentation in fluid particles trapped below the heat source.

Figure 11(a) and Figure 11(b) demonstrate the influence of the heater size on the mean distributions of gas temperature and velocity, respectively. It is essential to note that there is practically no impact of the source size on average velocity, whereas the mean temperature displays a quasi-linear and increasing profile. Furthermore, it should be observed that the radiation contribution leads to significantly higher temperature and velocity distributions. In Figure 11(c), the evolution of mean convection Nusselt numbers at the cavity surfaces is presented based on the heater aspect

ratio. Notably, the corresponding profiles are practically unaffected by the size of the heater, while the radiative contribution results in a slight amplification in the Nusselt numbers along the lower and side walls of the cavity. The impacts of the source aspect ratio on the average distributions of convection Nusselt numbers along the heater walls are depicted in Figure 11(d). It is evident that the corresponding trends reveal decreasing profiles, and more specifically, the $\overline{\mathrm{Nuc}}_{i2,3}$ trends show quasi-linear evolutions. It must be emphasized, however, that the $\overline{\mathrm{Nuc}}_{i1,4}$ values approach those of the $\overline{\mathrm{Nuc}}_{i2}$ as the upper wall of the enclosure is close to the upper wall of the heater. Moreover, the profiles of convection Nusselt numbers along the horizontal walls of the heater are practically unaffected by thermal radiation. Figure 11(e) and Figure 11(f) display the variations in average radiative Nusselt numbers with the heater aspect ratio. It is noteworthy that increasing the aspect ratio of the heater results in a rise in the average radiative Nusselt number along the walls of the enclosure. This can be attributed to the expansion of the heat source volume, leading to an enlargement of the heat-exchange surface area. Conversely, the radiative Nusselt numbers at the heater walls exhibit decreasing and quasi-linear trends. Additionally, it should be mentioned that the radiative Nusselt numbers at the heater sidewalls $\overline{\mathrm{Nur}}_{i1,4}$ approach those along the bottom heater wall $\overline{\mathrm{Nur}}_{i2}$ as the upper wall of the heater is positioned away from the upper surface of the enclosure. Figure 11(g) illustrates the evolution of the energy efficiency of the heating process with the heater size. It is noteworthy that despite the small variation in energy efficiency, opting for a square-shaped heater (AR=1) appears to be the most disadvantaged geometry, yielding the lowest heat transfer performance.

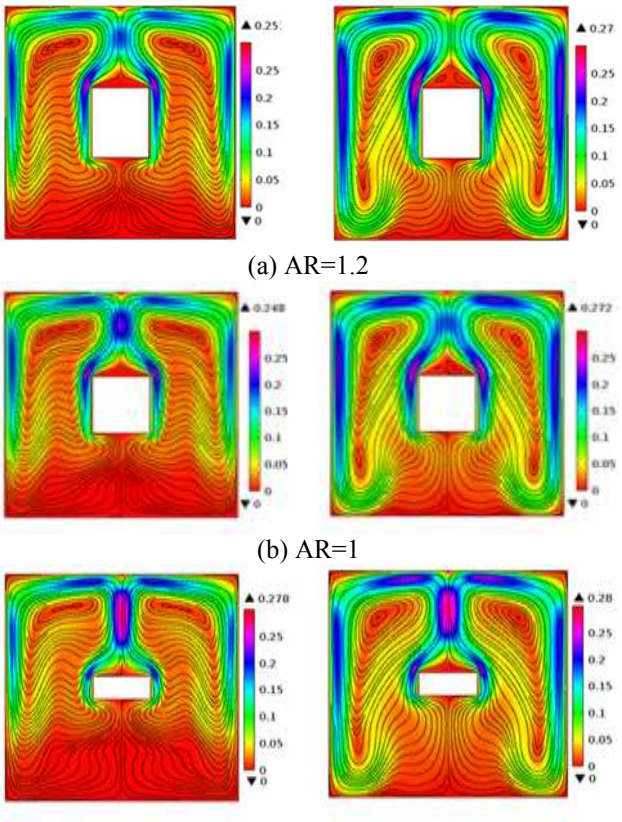

(a) AR=1.2

(b) AR=1

(c) AR=0.4

Fig. 9: Impact of the source size on the distributions of local velocity (m/s); without radiation (left); with radiation (right)
T_c=400K; T_h=800K; P=1atm; ε_c= ε_h=1; L_x=L_y=0.1m; L_{xx}=0.025m; P_{xx} =P_{yy}=0.0375m

4.4 Effect of the Source Location

The detailed analysis of the source location's effect on the behavior of flow structure and convective-radiative heating is presented in Figure 12 and Figure 13, respectively. Notably, the flow structure and the formation of fluid vortices are greatly influenced by the location of the heating element. In configuration "c", where the heater is positioned in the center of the enclosure, one can observe the formation of two symmetrical and counter-rotating convection cells close to the upper cavity wall. This change in the flow structure is accompanied by the development of a thermal plume originating from the heater.

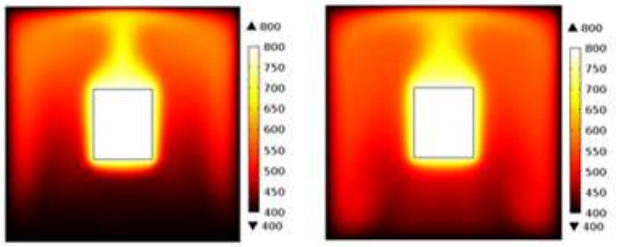

(a) AR=1.2

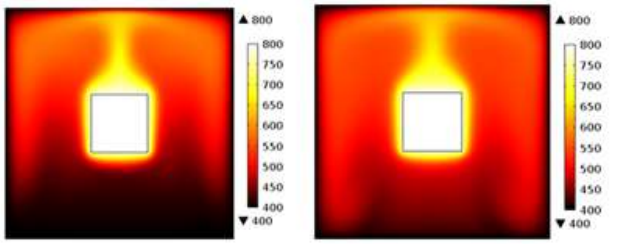

(b) AR=1

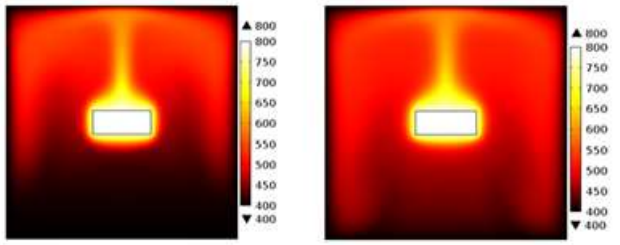

(c) AR=0.4

Fig. 10: Impact of the source size on the distributions of local temperature (K); without radiation (left); with radiation (right)
T_c=400K; T_h=800K; P=1atm; ε_c= ε_h=1; L_x=L_y=0.1m; L_{xx}=0.025m; P_{xx} =P_{yy}=0.0375m

Maximum velocities are localized at each top corner of the heat source, while high velocities are obtained above the heater and in the vicinity of the upper surface of the enclosure. An interesting aspect in cases where the source is situated close to the lower-left corner of the cavity (configuration "a") is the formation of a small recirculation cell above the heat source and another cell encompassing the rest of the cavity. When the source is situated close to the upper-right corner of the cavity (configuration "e"), the main finding is that the velocities of fluid particles at the upper corners of the heater are lower than those generated in the other configurations.

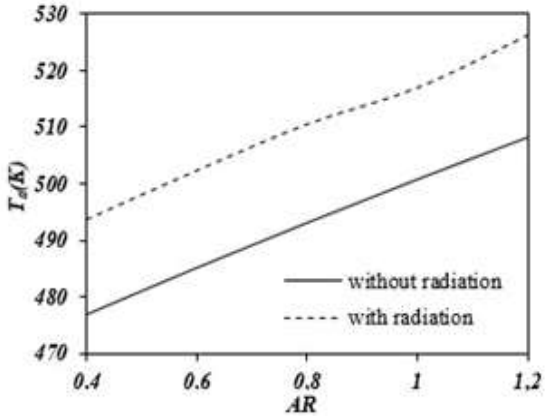

(a)

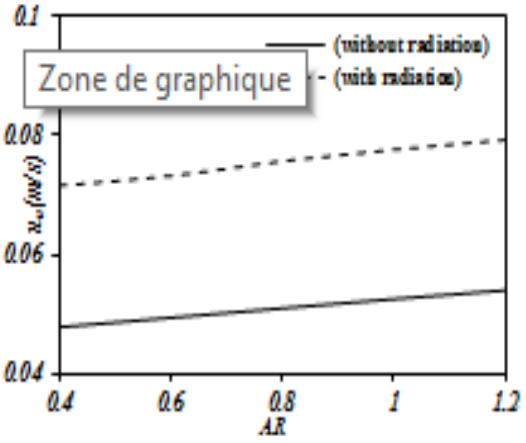

(b)

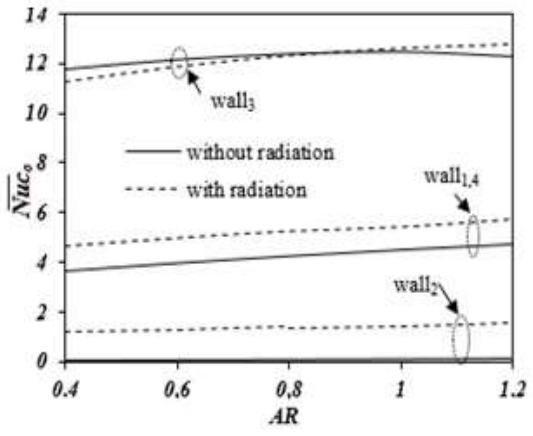

(c)

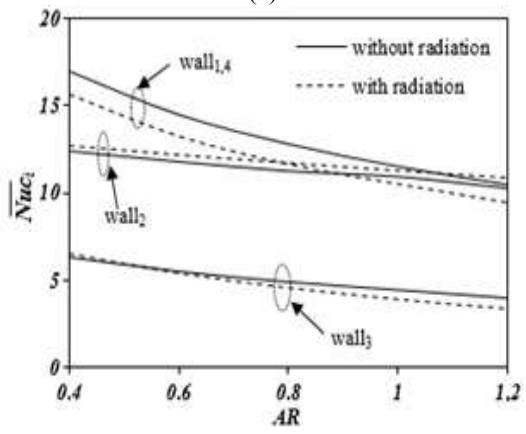

(d)

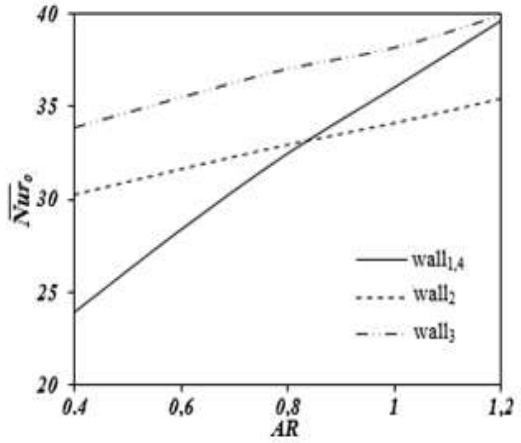

(e)

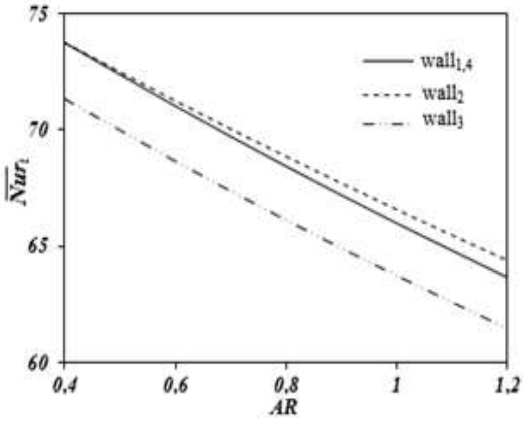

(f)

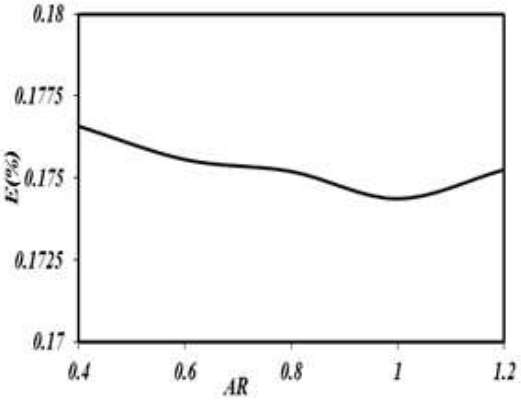

(g)

Fig. 11: Impact of the heater size on average distributions
T_h=800K; T_c=400K; P=1atm; ε_c= ε_h=1; L_x=L_y=0.1m; L_{xx}=0.025m; P_{xx} =P_{yy}=0.0375m

Furthermore, it should be pointed out that the radiative contribution homogenizes the temperature and increases fluid flow within the cavity. Specifically, the analysis of the radiative effect reveals significant local velocities when the heater is situated close to the bottom wall of the enclosure.

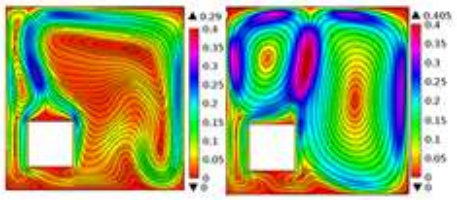

Configuration "a"

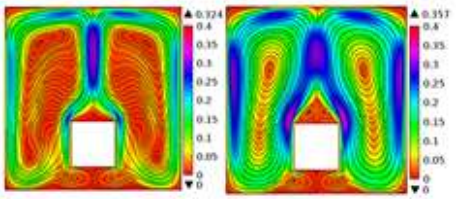

Configuration "b"

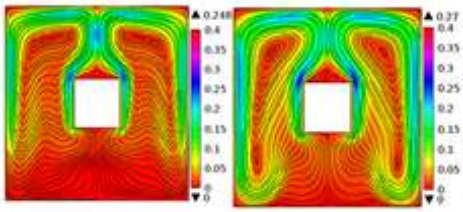

Configuration "c"

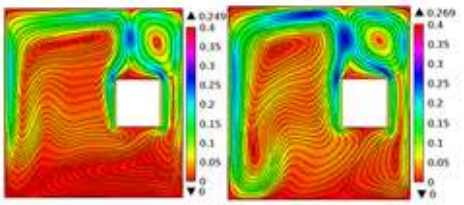

Configuration "d"

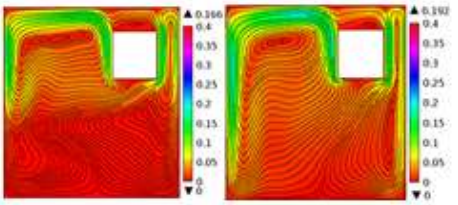

Configuration "e"

Fig. 12: Impact of the source location on local velocity profiles (m/s); without radiation (left); with radiation (right)
T_h=800K; T_c=400K; P=1atm; ε_c= ε_h=1; L_y=L_x=0.1m; L_{yy}=L_{xx}=0.025m; Configuration "a" P_{xx}=P_{yy} = 0.0125m; Configuration "b" P_{xx}= 0.0375m; P_{yy}=0.0125m; Configuration "c" P_{xx}=P_{yy}= 0.0375m; Configuration "d" P_{xx}=0.0625m, P_{yy}=0.0375m; Configuration "e" P_{xx}=P_{yy}=0.0625m.

Figure 14(a) and Figure 14(b) depict the variations in average temperature and velocity based on the heat source location. It is noteworthy that, independently of the radiative impact, the highest values of the mean temperature and velocity are attained when the source is situated at the bottom of the cavity. Moreover, radiation serves to homogenize the temperature fields within the cavity,

thereby increasing both mean velocity and temperature, with the exception of configuration "a" where the mean temperature in the absence of radiation is slightly higher than that computed with radiation.

Following Figure 14(c) and Figure 14(d), the higher values of $\overline{\mathrm{Nuc}}_{o1,2}$ are attained when the source is positioned close to the lower-left corner of the cavity (configuration "a"). Furthermore, it is noteworthy that the mean convection Nusselt number along the upper wall of the cavity $\overline{\mathrm{Nuc}}_{o3}$ reaches its maximum value when the heater is situated in the center of the enclosure.

This is logical since the structure and location of the fluid vortices generate large temperature gradients in the vicinity of the upper wall of the cavity. Furthermore, the higher values of $\overline{\mathrm{Nuc}}_{o4}$ are reached when the heater is situated at the center of the cavity and close to the sidewalls (configuration "d"). Regarding the radiative influence on the average convection Nusselt numbers along the heater walls shown in Figure 14(e) and Figure 14(f), it is notable that the distributions of the Nusselt numbers computed along the sidewalls of the heater are attenuated, except for those in configuration "b". Figure 14(g) indicates that there is hardly any difference between the radiation Nusselt numbers of the cavity walls when the heater is situated at the center of the cavity, and therefore, the corresponding profiles are practically comparable. On the other hand, the radiation Nusselt numbers of the enclosure walls display inverted trends for configurations "a" and "e". This can be explained by the physical boundary conditions imposed on the boundary. It should be noted that the heater location has practically no influence on the radiative Nusselt numbers along the heater boundaries, as shown in Figure 14(h). The corresponding trends are practically comparable with a slight difference due to the radiative contribution of the gas. It is evident from Figure 14(i) that energy efficiency is most pronounced when the source is positioned at the center of the lower section of the cavity (configuration "b"). The circulation flow rate becomes more pronounced when the heater is situated at the bottom of the cavity. Furthermore, if the heater is placed at the center of the enclosure, this allows better gas circulation and heat transfer.

4.5 Effect of the Pressure

According to Table 2, decreasing the gas pressure leads to an increase in fluid density, subsequently causing a rise in the average temperature and velocity of the gas. Additionally, it should be noted that increasing the gas pressure affects the optical characteristics of the medium by enhancing its optical thickness. This, in turn, reduces wall-to-wall heat transfer, resulting in lower radiation Nusselt numbers.

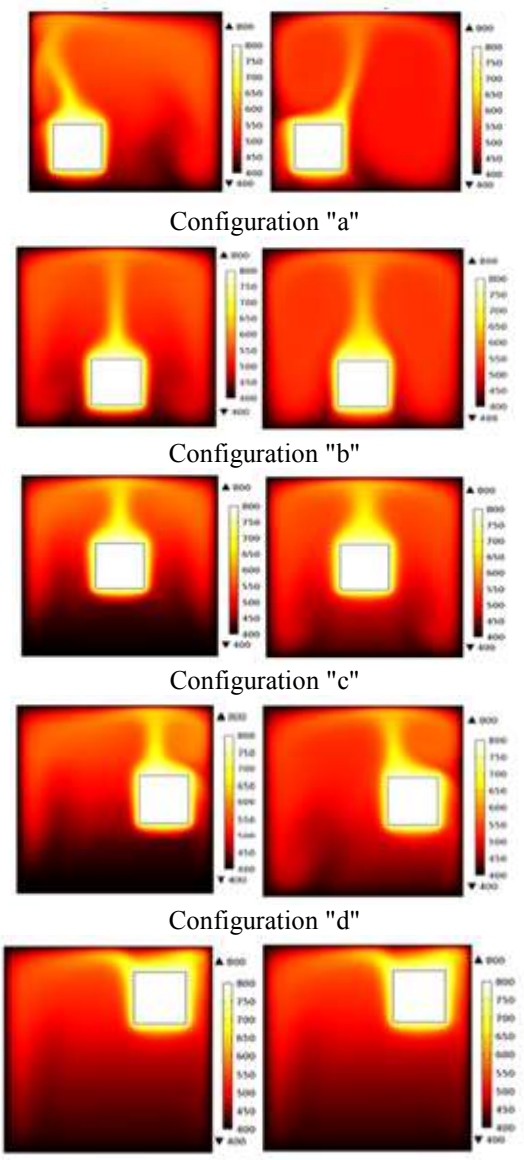

Fig. 13: Impact of the source location on local temperature profiles (K); without radiation (left); with radiation (right)
T_h=800K; T_c=400K; P=1atm; ε_c= ε_h=1; L_y=L_x=0.1m; L_{yy}=L_{xx}=0.025m; Configuration "a" P_{xx}=P_{yy} = 0.0125m; Configuration "b" P_{xx}= 0.0375m; P_{yy}=0.0125m; Configuration "c" P_{xx}=P_{yy}= 0.0375m; Configuration "d" P_{xx}=0.0625m, P_{yy}=0.0375m; Configuration "e" P_{xx}=P_{yy}=0.0625m.

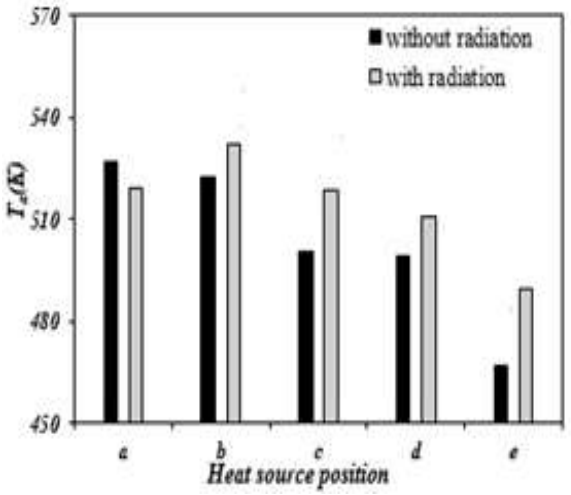

(a)

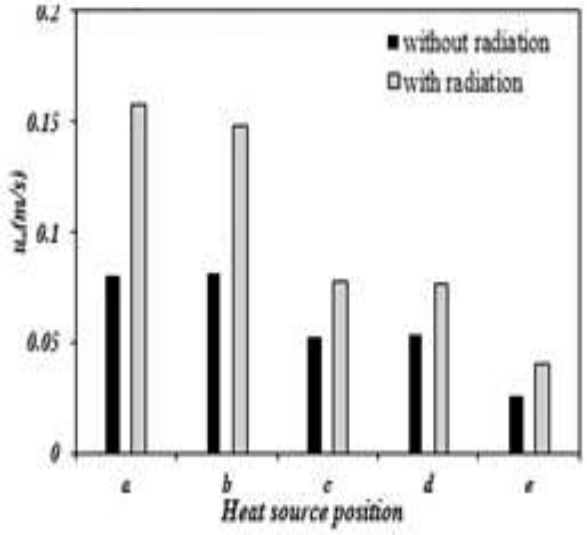

(b)

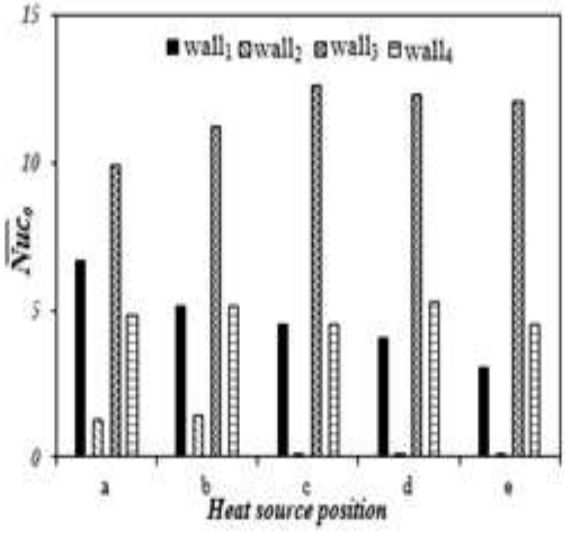

(c) without radiation

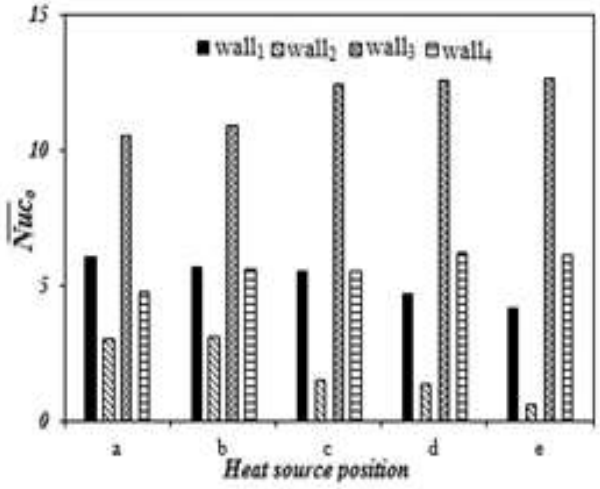

(d) with radiation

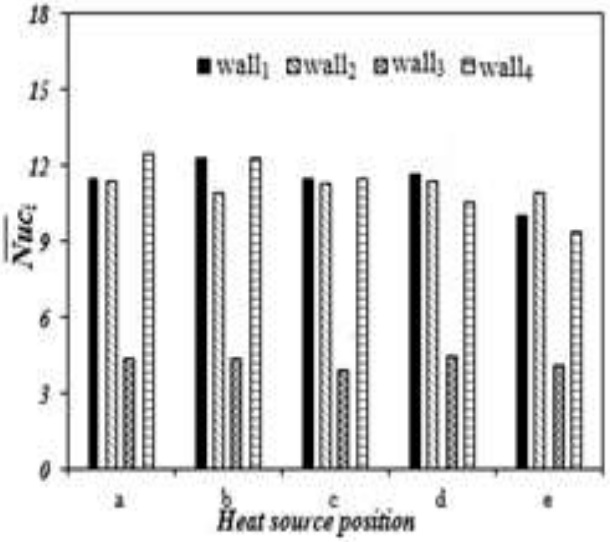

(e) without radiation

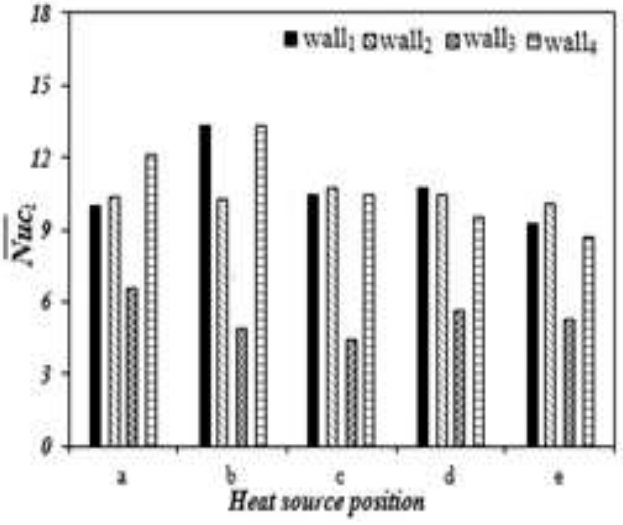

(f) with radiation

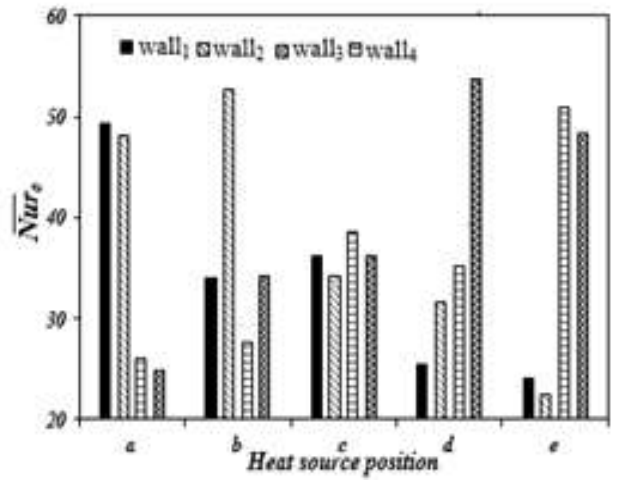

(g)

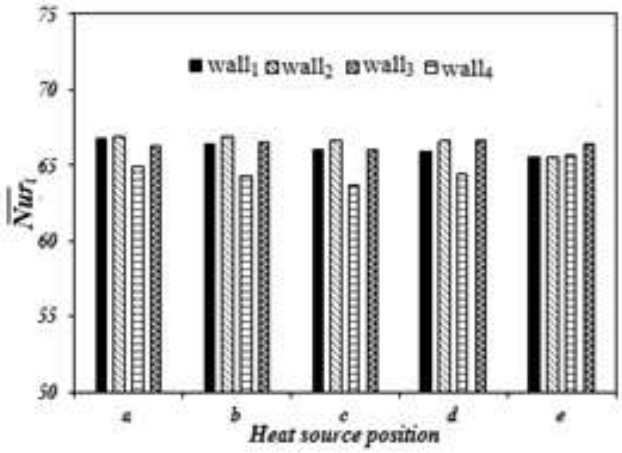

(h)

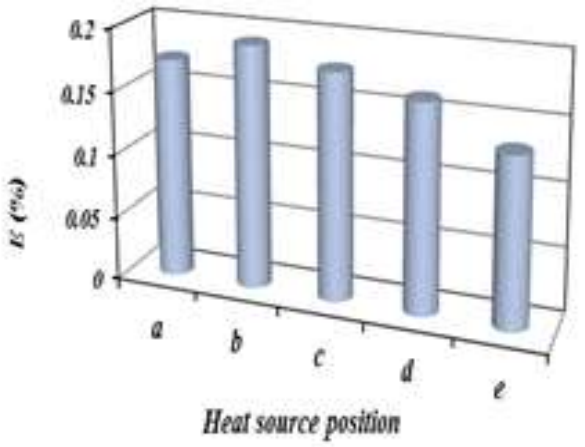

(i)

Fig. 14: Impact of the source location on average distributions
T_h=800K; T_c=400K; P=1atm; ε_c= ε_h=1; L_y=L_x=0.1m; L_{yy}=L_{xx}=0.025m; Configuration "a" P_{xx}=P_{yy} = 0.0125m; Configuration "b" P_{xx}= 0.0375m; P_{yy}=0.0125m; Configuration "c" P_{xx}=P_{yy}= 0.0375m; Configuration "d" P_{xx}=0.0625m, P_{yy}=0.0375m; Configuration "e" P_{xx}=P_{yy}=0.0625m

Table 2. Pressure effect (T_h=800K; T_c=400K; ε_c= ε_h=1; L_y=L_x=0.1m; L_{yy}=L_{xx}=0.025m; P_{yy} =P_{xx}=0.0375m)

		Pressure (atm)		
		1	2	3
Average temperature (K)	without radiation	500.80	494.47	491.46
	with radiation	517.10	515.26	513.60
Average velocity (m/s)	without radiation	0.052539	0.042285	0.036676
	with radiation	0.077609	0.068767	0.063864
Average radiative Nusselt numbers at the cavity walls	$Wall_{1,4}$	35.002	33.091	31.851
	$Wall_2$	33.080	30.142	28.249
	$Wall_3$	37.194	36.257	35.542
Average radiative Nusselt numbers at the heat source walls	$Wall_{1,4}$	63.696	62.290	61.450
	$Wall_2$	64.277	63.114	62.352
	$Wall_3$	125.06	120.15	116.83

5 Conclusion

Maximizing energy efficiency in thermal processes is crucial, necessitating the identification of the most effective setup for realizing optimal heat transfer performance. The present study delves into the impact of a heat-generating body on coupled thermal radiation and free convection in a square enclosure. The FT_{40} discrete-ordinate approximation, coupled with the (SNBcK) model, is applied to assess thermal radiation heat transfer. The findings indicate that thermal radiation significantly influences fluid flow and heat transfer by accelerating fluid vortices and homogenizing gas temperature. An elevation in the source temperature results in a considerable rise in gas temperature and a robust acceleration in flow rate. Furthermore, with an increase in the emissivity of the enclosure walls, the average gas temperature is significantly reduced, while the mean velocity profile remains almost unchanged. The study also reveals that increasing the heater aspect ratio enhances the mean temperature of the medium. Additionally, the results illustrate that maximum energy efficiency is attained when the source is positioned at the center of the lower section of the cavity.

Future investigations will be dedicated to the evaluation of thermodynamic irreversibility and entropy creation resulting from heat transfer, thereby enhancing the efficiency and performance of our heating process through the application of entropy minimization techniques.

References:

[1] El-Sadi H., Haghighar F. and Fallahi A., CFD Analysis of Turbulent Natural Ventilation in Double-Skin Façade: Thermal Mass and Energy Efficiency, *Journal of Energy Engineering,* Vol.136, No.3, 2010, pp. 68-75.

[2] Minko K.B. and Nashchekin M.D., Thermal performance of a metal hydride reactor for hydrogen storage with cooling/heating by natural convection, *Energy Storage and Saving*, 2023, Article in press.

[3] Fusegi T., Hyun J.M. and Kuwahara K., Natural convection in a differentially heated square cavity with internal heat generation, *Numerical Heat Transfer, Part A: Application,* Vol.21, No.2, 1992, pp. 215–229.

[4] Liu Y. and Phan-Thien N., A complete conjugate conduction convection and radiation problem for a heated block in a vertical differentially heated square enclosure, *Computional Mechanics,* Vol. 24, 1999, pp. 175–186.

[5] Bouali H., Mezrhab A., Amaoui H. and Bouzidi M., Radiation-natural convection heat transfer in an inclined rectangular enclosure, *International Journal of Thermal Sciences,* Vol.45, No.6, 2006, pp. 553-566.

[6] Kim B.S., Lee D.S., Ha M.Y., and Yoon H.S., A numerical study of natural convection in a square enclosure with a circular cylinder at different vertical locations, *International Journal of Heat and Mass Transfer,* Vol.51, No.7-8, 2008, pp. 1888–1906.

[7] Saha S., Saha G., and Islam M.Q., Natural convection in square enclosure with adiabatic cylinder at center and discrete bottom heating, *Daffodil International University Journal of Science and Technology,* Vol.3, No.1, 2008, pp. 29-36.

[8] Sun H., Chénier E., and Lauriat G., Effect of surface radiation on the breakdown of steady natural convection flows in a square, air-filled cavity containing a centered inner body, *Applied Thermal Engineering,* Vol.31, No.6-7, 2011, pp. 1252–1262.

[9] Sheikholeslami M., Gorji-Bandpay M. and Ganji D.D., Magnetic field effects on natural convection around a horizontal circular cylinder inside a square enclosure filled with nanofluid, *International Communications in Heat and Mass Transfer,* Vol. 39, No.7, 2012, pp. 978–986.

[10] Mahmoudi A.H. and Hooman K., Effect of a discrete heat source location on entropy generation in mixed convective cooling of a nanofluid inside the ventilated cavity, *International Journal of Exergy,* Vol.13, No.3, 2013, pp. 299-319.

[11] Saravanan S. and Sivaraj C., Coupled thermal radiation and natural convection heat transfer in a cavity with a heated plate inside, *International Journal of Heat and Fluid Flow,* Vol.40, 2013, pp. 54–64.

[12] Berrahil F., Benissaad S., Chérifa A. and Médale M., Natural convection with volumetric heat generation and external magnetic field in differentially heated enclosure, *Proceedings of Institution of Mechanical Engineers, Part C: Journal of Mechanical Engineering Science,* Vol. 228, No.15, 2014, pp. 2711-2727.

[13] Moortyh M.B.K., Kannan T., and Senthilvadivu K., Effects of Radiation on Free Convection Flow past an Upward Facing Horizontal Plate in a Nanofluid in the Presence of Internal Heat Generation. *WSEAS Transactions on Heat and Mass Transfer*, Vol. 10, 2015, pp. 9-20.

[14] Nagarajan N. and Periyasamy U., Natural Convection in a Tilted Square Enclosure Having Heat Generating Solid Body and with Various Thermal Boundaries, *Procedia Engineering,* Vol.127, 2015, pp. 1235 – 1242.

[15] Nguyen M.T., Aly A.M., and Lee S.W., Unsteady natural convection heat transfer in a nanofluid-filled square cavity with various heat source conditions, *Advances in Mechanical Engineering,* Vol. 8, 2016, pp. 1-18.

[16] Mun G.S., Doo J.H., and Ha M.Y., Thermo-dynamic irreversibility induced by natural convection in square enclosure with inner cylinder, Part-I: Effect of tilted angle of enclosure, *International Journal of Heat and Mass Transfer,* Vol.97, 2016, pp. 1102–1119.

[17] Doo J.H., Mun G.S., Ha M.Y., and Seong S.Y., Thermo-dynamic irreversibility induced by natural convection in square enclosure with inner cylinder. Part-II: Effect of vertical position of inner cylinder, *International Journal of Heat and Mass Transfer,* Vol.97, 2016, pp. 1120–1139.

[18] Pandey S., Park Y.G., and Ha M.Y., An exhaustive review of studies on natural convection in enclosures with and without internal bodies of various shapes, *International Journal of Heat and Mass Transfer,* Vol.138, 2019, pp. 762-795.

[19] Sivaraj C., Miroshnichenko I.V., and Sheremet M.A., Influence of thermal radiation on thermogravitational convection in a tilted chamber having heat-producing solid body, *International Communications in Heat and Mass Transfer,* Vol.115, 2020, pp. 104611.

[20] Dogonchi A.S., Tayebi T., Chamkha A.J. and Ganji D.D., Natural convection analysis in a

square enclosure with a wavy circular heater under magnetic field and nanoparticles, *Journal of Thermal Analysis and Calorimetry,* Vol.139, 2020, pp. 661-671.

[21] Hidki R., El Moutaouakil L., Boukendil M., Charqui Z., Zrikem Z. and Abdelbaki A., Natural convection coupled to surface radiation in an air-filled square cavity containing two heat-generating bodies, *Heat Transfer,* Vol. 52, No.3, 2023, pp. 2143-2164.

[22] Benhamou J., Lahmer E.B., Admi Y., Jami M. and Mezrhab A., Three-dimensional numerical simulation of free convection and entropy generation in a cubic cavity containing a heat source, *Heat Transfer,* Vol.52, No.7, 2023, pp. 5108-5135.

[23] Alsabery A.I., Kadhim H.T., Ismael M.A., Hashim I., and Chamkha A.J., Impacts of amplitude and heat source on natural convection of hybrid nanofluids into a wavy enclosure via heatline approach, *Waves in Random and complex media,* Vol.33, No.4, 2023, pp. 1060-1084.

[24] El Moutaouakil L., Boukendil M., Hidki R., Charqui Z., Zrikem Z. and Abdelbaki A., Analytical solution for natural convection of a heat-generating fluid in a vertical rectangular cavity with two pairs of heat source/sink, *Thermal Science and Engineering Progress*, Vol.40, 2023, 101738.

[25] Ben Nejma F., Mazgar A. and Charrada K., Volumetric and wall non grey gas entropy creation in a cylindrical enclosure, *WSEAS Transactions on Heat and Mass Transfer,* Vol.5, No.4, 2010, pp. 217-226.

[26] Saky A., Mazgar A., Slimi K. and Ben Nejma F., Thermal radiation contribution on humidification process in a cylindrical annular duct, *High Temperatures-High Pressures,* Vol.44, No.3, 2015, pp. 163-186.

[27] Mazgar A. and Ben Nejma F., Combined effect of natural convection and non-gray gas radiation with partial heating, *Sādhanā,* Vol.41, No.7, 2016, pp. 805-815.

[28] Ouertatani N., Ben Cheikh N., Ben Beya B., and Lili T., Numerical simulation of two-dimensional Rayleigh-Bénard convection in an enclosure, *Comptes Rendus Mécanique,* Vol.339, No.5, 2008, pp. 464-470.

[29] Goutiere V., Liu F. and Charette A., An assessment of real-gas modeling in 2D enclosures, *Journal of Quantitative Spectroscopy Radiative Transfer,* Vol.64, No.3, 2000, pp. 299–326.

[30] Borjini M.N., Guedri K., and Said R., Modeling of radiative heat transfer in 3D complex boiler with non-gray sooting media, *Journal of Quantitative Spectroscopy Radiative Transfer,* Vol.105, No.2, 2007, pp. 167-179.

Contribution of Individual Authors to the Creation of a Scientific Article (Ghostwriting Policy)

- Akram Mazgar prepared and wrote the manuscript. He also contributed to the numerical simulation of the physical problem on COMSOL software and the verification of the overall research outputs.
- Fadhila Hajji realized the iterative simulation on Matlab software and contributed to the numerical simulation of the physical problem on COMSOL software.
- Fayçal Ben Nejma used COMSOL Multiphysics® to model the physical problem. He also verified the overall research outputs.

The authors equally contributed to the present research, at all stages from the formulation of the problem to the final findings and solution.

Sources of Funding for Research Presented in a Scientific Article or Scientific Article Itself

No funding was received for conducting this study.

Conflict of Interest

The authors have no conflicts of interest to declare.